Applied Surface Science 538 (2021) 148064

Contents lists available at ScienceDirect

Applied Surface Science

journal homepage: www.elsevier.com/locate/apsusc

Stable Janus $TaSe_2$ single-layers via surface functionalization

Z. Kahraman[a], M. Baskurt[a], M. Yagmurcukardes[b,*], A. Chaves[c], H. Sahin[a]

[a] Department of Photonics, Izmir Institute of Technology, 35430 Izmir, Turkey
[b] Department of Physics, University of Antwerp, Groenenborgerlaan 171, B-2020 Antwerp, Belgium
[c] Universidade Federal do Ceara, Departamento de Fisica, Caixa Postal 6030, 60455-760 Fortaleza, Ceara, Brazil

ARTICLE INFO

Keywords:
Density functional theory
TaSe2
Janus single-layers
asymmetric surface functionalization

ABSTRACT

First-principles calculations are performed in order to investigate the formation of Janus structures of single-layer $TaSe_2$. The structural optimizations and phonon band dispersions reveal that the formation and stability of hydrogenated ($HTaSe_2$), fluorinated ($FTaSe_2$), and the one-side hydrogenated and one-side fluorinated (Janus-$HTaSe_2F$) single-layers are feasible in terms of their phonon band dispersions. It is shown that bare metallic single-layer $TaSe_2$ can be turned into a semiconductor as only one of its surface is functionalized while it remains as a metal via its two surfaces functionalization. In addition, the semiconducting nature of single-layers $HTaSe_2$ and $FTaSe_2$ and the metallic behavior of Janus $TaSe_2$ are found to be robust under applied uniaxal strains. Further analysis on piezoelectric properties of the predicted single-layers reveal the enhanced in-plane and out-of-plane piezoelectricity via formed Janus-$HTaSe_2F$. Our study indicates that single-layer $TaSe_2$ is a suitable host material for surface functionalization via fluorination and hydrogenation which exhibit distinctive electronic and vibrational properties.

1. Introduction

Recent progress in two dimensional (2D) ultra-thin crystals has been growing exponentially since the discovery of graphene, the first demonstrated 2D material [1,2]. The lack of a band gap in graphene, which limits its possible applications in optoelectronics, has made the search for other novel 2D materials inevitable. In order to overcome this problem, a wide range of 2D materials such as transition metal dichalcogenides (TMDs) [3–12], Xenes [13–19], have been successfully added to 2D library. In addition to TMDs and Xenes, which possess metallic, semi-metallic, or semiconducting behaviors, 2D insulators [20–22] have also been demonstrated and proposed as suitable candidates for heterostructure formations. 2D forms of TMDs have been the focus of interest of the scientific community due to their potential in applications such as ultra-sensitive photodetector [23], hydrogen evolution reaction [24,25], bio and chemical sensors [26–31].

Layered $TaSe_2$, a recent member of TMDs family, has been recently attracting great attention since its successful isolation from bulk structure [32]. Molecular-beam-epitaxy (MBE) has been shown to be an efficient technique for the growth of single-layer of $TaSe_2$ [33]. Raman spectroscopy experiments demonstrated that the two Raman active phonon modes, E_{2g} and A_{1g} of single-layer $TaSe_2$ are important for the characterization of its ultra-thin nature [34]. In addition to Raman spectroscopy, optical microscopy was shown to be useful for the identification of the layer number in $TaSe_2$ [35]. Moreover, it was proposed that single-layer $TaSe_2$ also exhibits charge-density-wave state [36].

The 2D nature of ultra-thin materials allows their surface functionalization, which has been shown to be an efficient way for tuning of their properties [37–39]. It has been experimentally demonstrated that the fluorination of surfaces of 2D materials can lead to tunable electronic, optical and mechanical properties [40–43]. For instance, as compared to bare graphene, fluorinated graphene has been announced to be more effective for catalysts in oxygen reduction reaction (ORR) [44,45]. On the other hand, hydrogen was also considered commonly in the functionalization of 2D surfaces that it can naturally occur in the experiments [46]. It has been shown that the band gap of graphene can be adjusted by functionalization of its one or both surfaces [47]. Therefore, the use of F and H atoms as the source for chemical functionalization of 2D materials allow researchers to demonstrate materials with diverse properties [48–51]. Moreover, using different type adatoms on different surfaces reveal also the formation of Janus type polar single-layers which have been shown to exhibit unique properties arising from the build-in electric field in the structure [52–57].

In this study, we investigated the formation of functionalized $TaSe_2$ structures using F and H atoms either on one surface or on both surfaces. The structural optimizations and phonon band diagrams reveal

* Corresponding author.
E-mail addresses: zeynepkahraman@iyte.edu.tr (Z. Kahraman), mehmetyagmurcukardes.edu@gmail.com (M. Yagmurcukardes).

https://doi.org/10.1016/j.apsusc.2020.148064
Received 26 June 2020; Received in revised form 21 September 2020; Accepted 3 October 2020
Available online 16 October 2020
0169-4332/

the formation of stable single-layers of $HTaSe_2$, $FTaSe_2$, and Janus-$HTaSe_2F$. It was shown that while one-side functionalized $TaSe_2$ structures turn into semiconductor, the Janus-$HTaSe_2F$ preserves the metallic nature of single-layer $TaSe_2$. In addition, all three single-layers were found to be robust against applied uniaxial strains by means of their electronic properties.

2. Computational details

All calculations were performed using the generalized gradient approximation (GGA) was adopted to describe the electron exchange and correlation in the Perdew-Burke-Ernzerhof (PBE) as implemented in the Vienna *ab initio* Simulation Package (VASP) [58,59]. The van der Waals (vdW) correction to the GGA functional was included by using the DFT-D2 method of Grimme [60]. Electronic band dispersions were calculated using GGA and the Heyd-Scuseria-Ernzerhof (HSE06) functionals, respectively in order to increase the accuracy of electronic structure calculations [61]. Analysis of the charge transfers in the structure was determined by the Bader technique [62].

For all calculations, a plane-wave basis set with a kinetic energy cutoff of 520 eV was used. For the structural optimization, the convergence criterion of the total force on the atoms in the primitive cell was reduced to 10^{-5} eV/Å while the convergence criterion for the energy was set to 10^{-6} eV. In order to eliminate interaction between the neighboring layers, a vacuum space of at least 20 Å was inserted. A Γ centered *k*-point mesh of 24 × 24 × 1 was used for the primitive cell optimization and it was increased to 48 × 48 × 1 for density of states (DOS) calculations.

The cohesive energy per unit cell was calculated using the formula $E_{Coh} = [\sum n_{atom}E_{atom} - E_{ML}]/n_{tot}$, where E_{atom} represents the energy of a single isolated atom while E_{ML} represents the total energy of the system. In addition, n_{tot} and n_{atom} denote the total number of atoms in the primitive unitcell and the number of atom of each type within the unitcell, respectively. The dynamical stability of each structure was evaluated by calculating their phonon band dispersion through the whole Brillouin Zone (BZ) using the PHONOPY code, which uses the small displacement methodology [63].

3. Results

3.1. Structural properties

One of the structural phases of $TaSe_2$ is known as the hexagonal 2H-phase which consists of stacked $TaSe_2$ layers. In a single-layer of hexagonal $TaSe_2$, Ta-layer is sandwiched between two Se-layers which are separated symmetrically with respect to the Ta-layer in the out-of-plane direction. Once the $TaSe_2$ surface is functionalized, the structural phase is conserved while the symmetry along the out-of-plane direction is broken. Therefore, the optimized lattice parameters, the bond lengths etc…are comparable to each other in each single-layer structure.

The side views of optimized structures of each single-layer are presented in Fig. 1. As listed in Table 1, atomic adsorption on each Se site enlarges the lattice in the in-plane directions. The optimized lattice parameters for bare $TaSe_2$ (3.48 Å) expands to 3.55 Å for $HTaSe_2$ and it expands to 3.57 Å for $FTaSe_2$ and Janus $HTaSe_2F$. Moreover, the atomic bond length between Ta-Se atoms in bare $TaSe_2$ (2.61 Å) becomes different for two sides of the layer via functionalization. In single-layer $HTaSe_2$, the atomic bond length between Ta atom and Se atom which binds to H is 2.56 Å while Ta-Se bond length is 2.64 Å on the other surface. Similarly, in single-layer $FTaSe_2$ two Ta-Se bond lengths are found, 2.52 and 2.64 Å from functionalized and bare surfaces, respectively. In the Janus structure two Ta-Se bond lengths, 2.61 and 2.57 Å for H and F sides, respectively, are found. The functionalization of $TaSe_2$ breaks the structural symmetry with respect to the Ta-layer. In addition to symmetry breaking, different amount of charge depletions on each surface also induces internal polarization in the functionalized

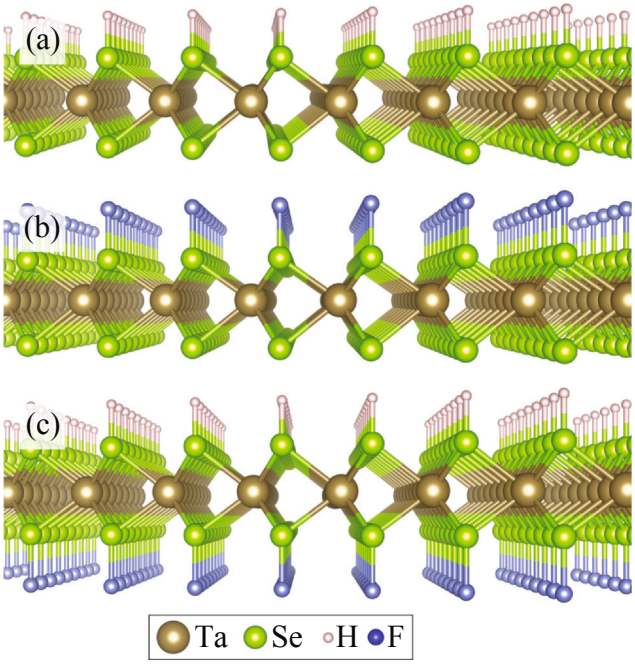

Fig. 1. Perspective views of single-layers (a) $HTaSe_2$, (b) $FTaSe_2$, and (c) Janus $HTaSe_2F$. The colors representing each atom are given below. (For interpretation of the references to colour in this figure legend, the reader is referred to the web version of this article.)

structures. Furthermore, the calculated cohesive energies per formula reveal that the functionalized structures have lower cohesive energies than that of the bare $TaSe_2$. It is found that the formation of fluorinated surface is more energetic than the formation of hydrogenated surface, which can be attributed to strong F-Se bonding. Apparently, the structural changes are dominated by the fluorinated surface in Janus structure as a consequence of large charge transfer between Se and F atoms.

3.2. Vibrational properties

The dynamical stability of each $TaSe_2$ single-layer structure is investigated in terms of the phonon band dispersions through the whole BZ as presented in Fig. 2. Note that the phonon bands are presented in the Fig. S1(a) of the Supporting Information. Apparently, the phonon branches are almost free from any imaginary eigenfrequencies indicating the dynamical stability of the structures. The optical phonon branches at the Γ point of the BZ are classified as non-degenerate out-of-plane and doubly-degenerate in-plane modes due to in-plane structural isotropy.

As shown in Fig. S2, single-layer $HTaSe_2$ exhibits three doubly-degenerate in-plane and three non-degenerate out-of-plane phonon modes. The lowest frequency in-plane mode (156 cm^{-1}) is attributed to the out-of-phase vibration of bottom Se and top Se-H pairs against each other. The in-plane phonon mode at frequency 231 cm^{-1} originates from in-phase vibration of two Se and H atomic layers against Ta-layer. In addition, the doubly-degenerate mode having frequency 437 cm^{-1} denotes the in-plane stretching of H atoms. On the other hand, one of the out-of-plane modes of $HTaSe_2$, having frequency 2120 cm^{-1}, originates from the pure Se-H bond stretching. The mode at frequency 212 cm^{-1} is attributed to the breathing-like vibration of top-Se-H and lower-Se-Ta pairs against each other while the mode having frequency 265 cm^{-1} denotes the out-of-phase vibration of Ta-layer and the Se-Se-H atomic layers.

The Fig. 2(b) represents the phonon band dispersions of single-layer $FTaSe_2$ for which the same amount of in-plane and out-of-plane optical

Table 1
The calculated parameters for the single-layers of bare and functionalized $TaSe_2$ structures are: the optimized in-plane lattice constants, $a = b$; the atomic bond lengths between Ta-Se and Se-X atoms (X = F, H), d_{Ta-Se} and d_{Se-X}; the distance between the outermost atoms of single-layer, h; the cohesive energy per formula, E_{Coh}; the amount of change in the charge of each atom after structural optimization (signs + and − indicate excess and the lack of electron on the atom), $\triangle\rho$; magnetic ground state of the structure, and the electronic band gap calculated within GGA and HSE06 functionals, E_g^{GGA} and E_g^{HSE06}.

	$a = b$ (Å)	d_{Ta-Se} (Å)	d_{Se-H} (Å)	d_{Se-F} (Å)	h (Å)	E_{Coh} (eV)	$\triangle\rho_{Ta}$ (e^-)	$\triangle\rho_{Se}$ (e^-)	$\triangle\rho_F$ (e^-)	$\triangle\rho_H$ (e^-)	μ (−)	E_g^{GGA} (eV)	E_g^{HSE06} (eV)
$TaSe_2$	3.48	2.61	–	–	3.33	5.77	−1.4	+0.7/+0.7	–	–	NM	–	–
$HTaSe_2$	3.55	2.56/2.64	1.51	–	4.68	4.66	−1.2	+0.7/+0.4	–	+0.1	NM	0.77	1.19
$FTaSe_2$	3.57	2.52/2.64	–	1.81	4.92	4.96	−1.2	+0.6/+0.0	+0.6	–	NM	0.27	0.53
Janus $HTaSe_2F$	3.57	2.61/2.57	1.55	1.87	6.56	4.20	−1.1	+0.1/+0.4	+0.5	+0.1	NM	–	–

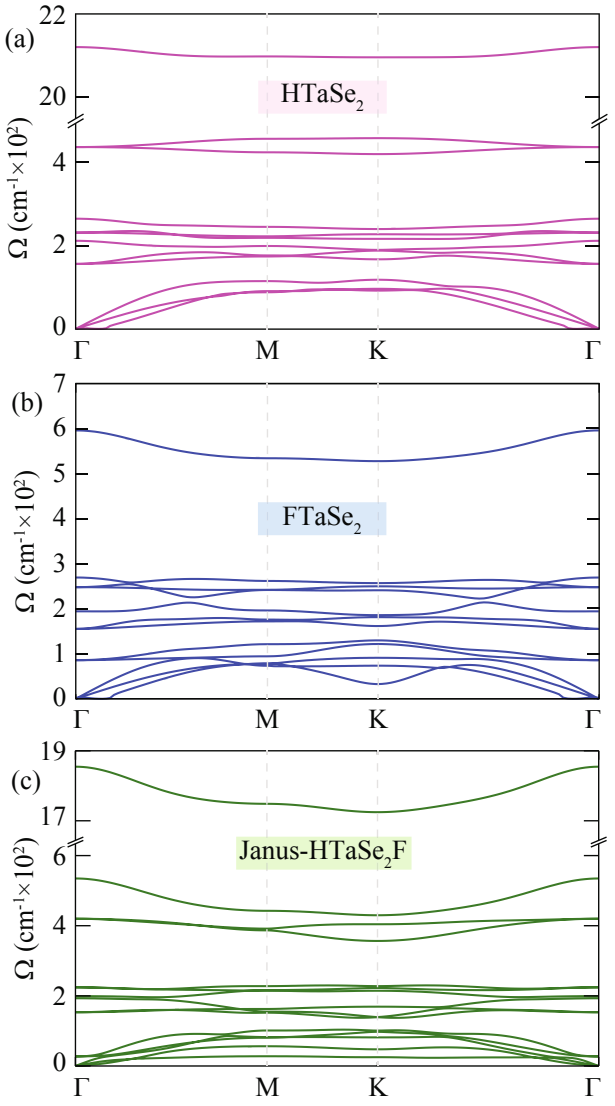

Fig. 2. Phonon band dispersions of single-layers (a) $HTaSe_2$, (b) $FTaSe_2$, and (c) Janus $HTaSe_2F$.

phonon branches exist as in the case of $HTaSe_2$. As presented in Fig. S2, three doubly-degenerate phonon modes of $FTaSe_2$ are found to be at 86, 155, and 248 cm^{-1}, respectively. The three modes represent the following vibrations; the opposite in-plane stretching F, the out-of-phase vibration of F-Se (Se from lower plane) and Ta-Se (Se from upper plane), and shear-like vibration of each atomic layer against each other, respectively. The frequencies of phonon modes in $FTaSe_2$ are smaller than those in $HTaSe_2$ as a direct consequence of stronger Ta-Se bonds in latter structure. Moreover, the out-of-plane phonon branches are calculated to be at 194, 269, and 596 cm^{-1}, respectively. The mode at 194 cm^{-1} represents the breathing-like vibration of F and $TaSe_2$ layers against each other while the mode at 269 cm^{-1} originates from vibration of Ta layer against the F-Se-Se layers. The other mode at 596 cm^{-1} is related with the opposite vibration of F and top-Se layers against each other.

In the Janus single-layer, there are additional phonon branches arising from two-side functionalization of the structure. The four in-plane doubly-degenerate modes are found to be at 153, 193, 224, and 420 cm^{-1} while the out-of-plane modes have frequencies 199, 535, and 1855 cm^{-1}. Notably, there are two out-of-plane modes at 199 cm^{-1} which only differ by 0.1 cm^{-1} and they are attributed to the out-of-phase vibration of Ta/H-Se-Se-F layers, and Ta-Se-F/Se-H atomic layers, respectively. The mode at 535 cm^{-1} represents the opposite vibrations of Se-H and Se-F couples against each other. The highest frequency out-of-plane mode originates from Se-H bond stretching as in single-layer $HTaSe_2$. The softening of its frequency in Janus structure can be related to the F-Se bond formation on the other surface that the H-Se bond length in Janus structure (1.55 Å) becomes larger than that of in $HTaSe_2$ (1.51 Å). The increase in the bond length results in the softening of the frequency of Se-H bond stretching.

3.3. Electronic properties

As reported for graphene, surface functionalization can be an efficient way for tuning the electronic properties of a 2D material. It has been demonstrated that hydrogenation leads to opening a band gap in graphene [64]. In addition, fluorination has also been shown to efficient for the band gap engineering of graphene sheet [65].

In the case of metallic $TaSe_2$ (see Fig. S1(b)), it is found that one-side hydrogenation or fluorination lead to the opening of a band gap as presented in Figs. 3(a) and (b). The electronic band gaps of single-layers $HTaSe_2$ and $FTaSe_2$ are calculated to be 0.77 and 0.27 eV, respectively. The electronic band gaps are also calculated by using HSE06 and the results are presented in Supporting Information and band gap values are given in Table 1. Notably, both single-layers are found to exhibit indirect gap behavior while the latter displaying also quasi-direct nature whose energy difference between two conduction band edges is ~30 meV. In both of the structures, occupation of Se-*p* orbitals via atomic functionalization results in shift of the bands around the Fermi level to low energies driving the metal-to-semiconductor transition. In contrast, as the both surface of $TaSe_2$ are functionalized, i.e. Janus structure is formed, the metallicity of $TaSe_2$ is found to be conserved as consequence of charge receive (donation) on F (H) sides that both conduction and valence band states shift and cross the Fermi level (see Fig. 3(c)).

3.4. Strain-dependent properties

Strain is often present in experiments either naturally or controllably and it can alter the electronic properties of materials. Usually in experiments, strain is applied by the help of substrate on which the

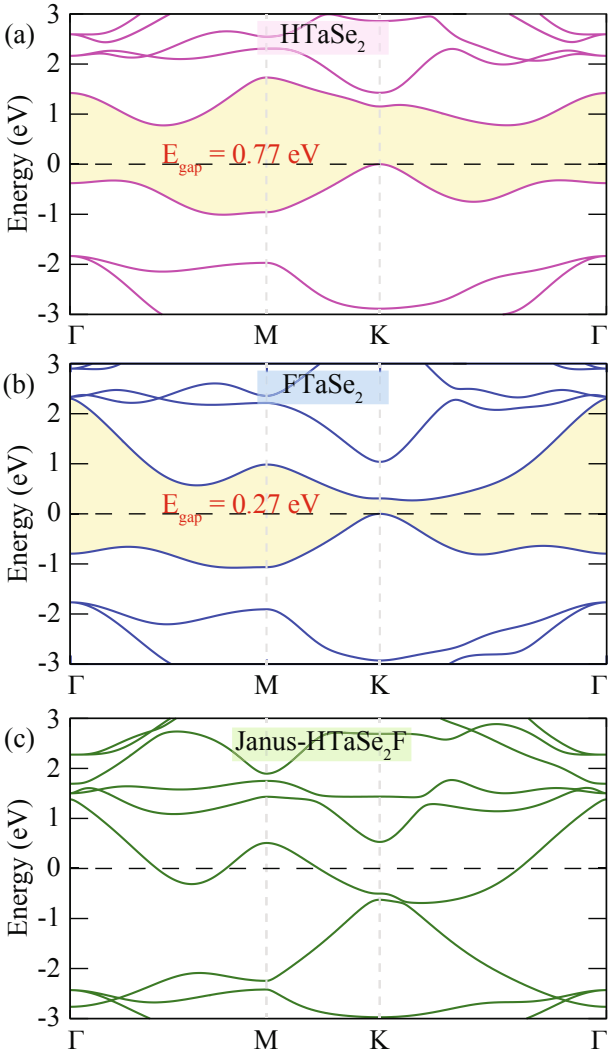

Fig. 3. Electronic band dispersions of single-layers (a) $HTaSe_2$, (b) $FTaSe_2$, and (c) Janus $HTaSe_2F$.

single layer material resides. By the bending of the substrate, an external strain can be applied on the 2D single layer [66,67]. For the semiconducting $HTaSe_2$, $FTaSe_2$ and metallic Janus single-layers, we investigate the effect of uniaxial strain on their electronic band dispersions. In order to simulate the uniaxial strain, a rectangular primitive unit cell is considered in which the armchair (AC) and zigzag (ZZ) directions are oriented along the *a* and *b* vectors, respectively. The strength of the applied strain is kept between ±5% with steps of 2% and the results of the strained electronic band dispersions are presented in Fig. 4. Note that, the strained electronic band structures are calculated using primitive rectangular unitcell for simplicity.

For the unstrained single-layer of $HTaSe_2$, the VBM and CBM are located in between the Γ-Y and Γ-X points of the rectangular BZ, respectively. As the uniaxial strain is applied along the AC orientation, the VBM is found to reside between the Γ-Y independent of the strength and type of the strain, tensile or compressive. The valence band edge residing between the Γ-X points displays a shift to the X point as the applied compressive strain increases while it exhibits a shift towards the Γ point as the applied tensile strain increases. In addition to the shifts, its energy decreases (increases) via the applied compressive (tensile) strains. Although, the indirect semiconducting nature of $HTaSe_2$ is robust, the CBM remains at the same point via tensile strain while it shifts from Γ-X to Γ-Y under compressive strain. A similar behavior is found for the two valence band edges residing between the Γ-X

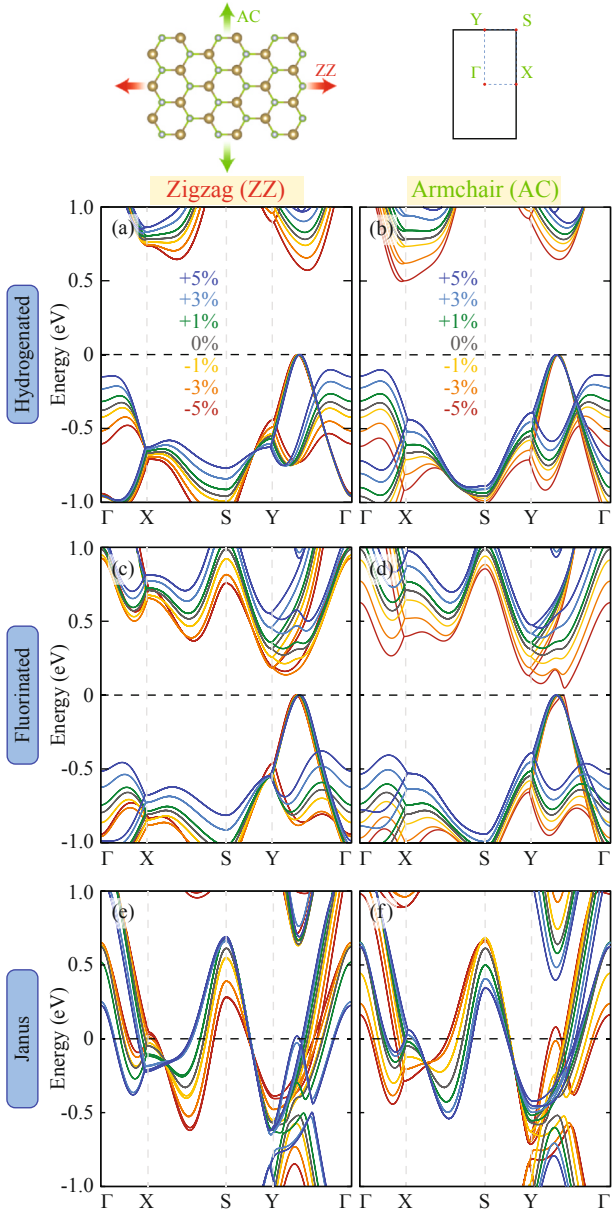

Fig. 4. Uniaxial strain-dependent electronic band dispersions of single-layer $HTaSe_2$ for (a) AC and (b) ZZ orientations. Those of single-layer $FTaSe_2$ for (c) AC and (d) ZZ orientations. (e) and (f) stand for the AC- and ZZ-strain dependent band dispersion of the Janus single-layer.

and Γ-Y for the strain applied along the ZZ orientation. However, energy of the conduction band edge located near the X point decreases with applied compressive strain indicating the shift of the CBM from Γ-Y. In addition, the flat bands between the X-S points become dispersive for both tensile and compressive strains indicating the deformation of localized states. Overall, it is found that single-layer $HTaSe_2$ exhibits robust indirect gap semiconducting behavior under applied uniaxal strain with changing energy gap.

The electronic band dispersions of unstrained single-layer $FTaSe_2$ in its rectangular primitive cell reveal that the VBM and CBM reside between the Y-Γ points. Although, the structure exhibits an indirect band gap behavior, the energy difference between two conduction band edges is found to be only 40 meV. As the uniaxial tensile strain is applied along the AC orientation, the energy difference between the two conduction band edges increases to 75 meV at 5% of strain. In contrast, with increasing compressive strain the energy difference decreases and

Table 2
The calculated parameters for single-layers of $TaSe_2$, $HTaSe_2$, $FTaSe_2$, and $HTaSe_2F$ are: in-plane stiffness, *C*; the relaxed-ion piezoelectric stress, e_{ij}; the corresponding piezoelectric strain coefficients, d_{ij}; and Poisson ratio, ν.

	C_{11} (Nm^{-1})	C_{12} (Nm^{-1})	C (Nm^{-1})	ν –	e_{11} ($Cm^{-1} \times 10^{-10}$)	e_{31} ($Cm^{-1} \times 10^{-10}$)	d_{11} (pmV^{-1})	d_{31} (pmV^{-1})
$TaSe_2$	99.1	34.7	87.0	0.35	2.58	0.00	4.00	0.00
$HTaSe_2$	79.1	17.8	75.0	0.22	1.97	0.08	3.21	0.09
$FTaSe_2$	70.8	13.0	68.0	0.18	0.96	0.62	1.66	0.74
$HTaSe_2F$	70.5	32.8	55.2	0.49	7.89	0.03	20.91	0.03

the CBM becomes a convex. It indicates that the quasi-direct band structure of single-layer $FTaSe_2$ disappears under compressive strain along AC orientation. In contrast to what we find for strain along AC direction, the energy difference between two conduction band edges increases via compressive strain along ZZ orientation while CBM becomes convex as the tensile strain increases. Although, the conduction band becomes convex as the tensile strain increases, the CBM shifts to the Y point and therefore, the indirect gap nature of the single-layer is conserved. Similarly, the Janus single-layer is found to be robust against the applied uniaxal strain by preserving its metallic behavior.

3.5. Elastic and piezoelectric properties

Using the knowledge of the elastic stiffness tensor, the in-plane stiffness (*C*) and the Poisson ratio (ν) can be investigated. As compared to the well-known 2D materials such as graphene (330 N/m) [68], and single-layer MoS_2 (122 N/m) [68], single-layer $TaSe_2$ possesses a soft nature indicated by its in-plane stiffness (99.1 N/m). Functionalization of $TaSe_2$ by hydrogenation and fluorination causes a softening in the bonding states of Ta-Se atoms and the in-plane stiffness values are found to decrease (79.1, 70.8, and 70.5 N/m for $HTaSe_2$, $FTaSe_2$, and Janus $HTaSe_2F$, respectively). In addition, the Poisson ratios are calculated to decrease (0.35 for $TaSe_2$) by one-surface functionalization (0.22 and 0.18 for $HTaSe_2$ and $FTaSe_2$) while it increases to 0.49 in Janus $HTaSe_2F$. The relatively high Poisson ratio of Janus $HTaSe_2F$ indicates its ability to retain its structure under external loads.

Piezoelectricity is a reversible physical process resulting from the electromechanical interaction between mechanical and electrical states in materials having inversion asymmetry, that is, an internal electric field can be created due to an applied mechanical stress or a mechanical stress caused by an applied electric field can be induced. Piezoelectric stress coefficients, e_{ij}, the parameters determining the piezoelectric properties, are the sum of ionic and electronic contributions, and piezoelectric strain constants, d_{ij}, are related to each other by elastic tensor elements, C_{ij}, as follows;

$$d_{11} = \left(\frac{e_{11}}{C_{11} - C_{12}}\right),$$
$$d_{31} = \left(\frac{e_{31}}{C_{11} + C_{12}}\right), \quad (1)$$

As listed in Table 2, e_{11} values are found to be 2.58×10^{-10} Cm^{-1} for bare $TaSe_2$, which is less than that of single-layer MoS_2 (3.88×10^{-10} Cm^{-1}) [68]. The single surface functionalization is shown to decrease e_{11} values to 1.97×10^{-10} Cm^{-1} and 0.96×10^{-10} Cm^{-1} for $HTaSe_2$ and $FTaSe_2$, respectively. In contrast, in the formed Janus $HTaSe_2F$ the e_{11} value is found to be 7.89×10^{-10} Cm^{-1} which is considerably large as compared to other $TaSe_2$ derivatives. The reason for such increase is the created charge asymmetry on both surfaces. In addition, the created charge asymmetry leads to the higher contribution of the ionic relaxation to the piezoelectricity. In contrast to bare $TaSe_2$, which has out-of-plane symmetry, in single-layers of $HTaSe_2$, $TaSe_2F$, and Janus $HTaSe_2F$ non-zero e_{31} elements are found arising from the induced dipole in the structure. e_{31} values are found to be 0.08, 0.62, and 0.03 for $HTaSe_2$, $TaSe_2F$, and Janus $HTaSe_2F$, respectively. Those results can directly be related to the total amount of charge depleted to the Se, F, and H atoms by Ta atoms as listed in Table 1. As the depleted charge difference between Se-F and Se-H pairs increases, the corresponding e_{31} values get larger which is the case for $HTaSe_2$. Moreover, piezoelectric strain coefficients are also listed in Table 2.

4. Conclusion

By performing state-of-the-art density functional theory calculations, we investigated the structural, vibrational, electronic, and piezoelectric properties of single-layer $TaSe_2$ structures constructed by its surface functionalization using H and F atoms. Our results revealed that the surface functionalization of $TaSe_2$ is energetically feasible and lead to dynamically stable Janus single-layer structures. As the one-surface of the $TaSe_2$ is functionalized, electronically it was shown that there exists a metallic-to-semiconductor transition for single-layer of $HTaSe_2$ and $FTaSe_2$ while by the both surface functionalization, i.e. in the Janus single-layer, the metallicity is conserved. Moreover, both the metallicity and semiconducting nature of Janus-$HTaSe_2F$ structures were shown to be robust against applied uniaxal strains. Further analysis on the elastic and piezoelectric tensors revealed that the induced dipole moment in the $TaSe_2$ derivatives creates out-of-plane piezoelectricity in the structures.

Declaration of Competing Interest

The authors declare that they have no known competing financial interests or personal relationships that could have appeared to influence the work reported in this paper.

acknowledgments

Computational resources were provided by TUBITAK ULAKBIM, High Performance and Grid Computing Center (TR-Grid e-Infrastructure). HS acknowledges support from Türkiye Bilimler Akademisi - Turkish Academy of Sciences under the GEBIP program. This work was supported by the Flemish Science Foundation (FWO-Vl) by a postdoctoral fellowship (M.Y.).

Appendix A. Supplementary material

Supplementary data associated with this article can be found, in the online version, at https://doi.org/10.1016/j.apsusc.2020.148064.

References

[1] K.S. Novoselov, A.K. Geim, S.V. Morozov, D. Jiang, Y. Zhang, S.V. Dubonos, I.V. Grigorieva, A.A. Firsov, Science 306 (2004) 666.
[2] A.K. Geim, K.S. Novoselov, Nanoscience and technology: a collection of reviews from nature journals (World Scientific, (2010), pp. 11–19.
[3] Q.H. Wang, K. Kalantar-Zadeh, A. Kis, J.N. Coleman, M.S. Strano, Nat. Nanotechnol. 7 (2012) 699.
[4] M. Chhowalla, H.S. Shin, G. Eda, L.-J. Li, K.P. Loh, H. Zhang, Nat. Chem. 5 (2013) 263.
[5] A. Ramasubramaniam, Phys. Rev. B 86 (2012) 115409.
[6] K.F. Mak, C. Lee, J. Hone, J. Shan, T.F. Heinz, Phys. Rev. Lett. 105 (2010) 136805.
[7] B. Radisavljevic, A. Radenovic, J. Brivio, V. Giacometti, A. Kis, Nat. Nanotechnol. 6 (2011) 147.

[8] S. Tongay, J. Zhou, C. Ataca, K. Lo, T.S. Matthews, J. Li, J.C. Grossman, J. Wu, Nano Lett. 12 (2012) 5576.
[9] T. Georgiou, R. Jalil, B.D. Belle, L. Britnell, R.V. Gorbachev, S.V. Morozov, Y.-J. Kim, A. Gholinia, S.J. Haigh, O. Makarovsky, et al., Nat. Nanotechnol. 8 (2013) 100.
[10] H. Fang, S. Chuang, T.C. Chang, K. Takei, T. Takahashi, A. Javey, Nano Lett. 12 (2012) 3788.
[11] J.S. Ross, P. Klement, A.M. Jones, N.J. Ghimire, J. Yan, D. Mandrus, T. Taniguchi, K. Watanabe, K. Kitamura, W. Yao, et al., Nat. Nanotechnol. 9 (2014) 268.
[12] S. Tongay, H. Sahin, C. Ko, A. Luce, W. Fan, K. Liu, J. Zhou, Y.-S. Huang, C.-H. Ho, J. Yan, et al., Nat. Commun. 5 (2014) 3252.
[13] A. Molle, J. Goldberger, M. Houssa, Y. Xu, S.-C. Zhang, D. Akinwande, Nat. Mater. 16 (2017) 163.
[14] L. Matthes, O. Pulci, F. Bechstedt, New J. Phys. 16 (2014) 105007.
[15] H. Sahin, S. Cahangirov, M. Topsakal, E. Bekaroglu, E. Akturk, R.T. Senger, S. Ciraci, Phys. Rev. B 80 (2009) 155453.
[16] P. Vogt, P. De Padova, C. Quaresima, J. Avila, E. Frantzeskakis, M.C. Asensio, A. Resta, B. Ealet, G. Le Lay, Phys. Rev. Lett. 108 (2012) 155501.
[17] M. Dávila, L. Xian, S. Cahangirov, A. Rubio, G. Le Lay, New J. Phys. 16 (2014) 095002.
[18] F.-F. Zhu, W.-J. Chen, Y. Xu, C.-L. Gao, D.-D. Guan, C.-H. Liu, D. Qian, S.-C. Zhang, J.-F. Jia, Nat. Mater. 14 (2015) 1020.
[19] X.-L. Yu, L. Huang, J. Wu, Phys. Rev. B 95 (2017) 125113.
[20] C. Jin, F. Lin, K. Suenaga, S. Iijima, Phys. Rev. Lett. 102 (2009) 195505.
[21] M. Baskurt, J. Kang, H. Sahin, Phys. Chem. Chem. Phys. 22 (2020) 2949.
[22] M. Baskurt, M. Yagmurcukardes, F.M. Peeters, H. Sahin, J. Chem. Phys. 152 (2020) 164116.
[23] K.S. Kim, Y.J. Ji, K.H. Kim, S. Choi, D.-H. Kang, K. Heo, S. Cho, S. Yim, S. Lee, J.-H. Park, et al., Nat. Commun. 10 (2019) 1.
[24] Y. He, P. Tang, Z. Hu, Q. He, C. Zhu, L. Wang, Q. Zeng, P. Golani, G. Gao, W. Fu, et al., Nat. Commun. 11 (2020) 1.
[25] D. Krasnozhon, D. Lembke, C. Nyffeler, Y. Leblebici, A. Kis, Nano Lett. 14 (2014) 5905.
[26] S. Barua, H.S. Dutta, S. Gogoi, R. Devi, R. Khan, A.C.S. Appl, Nano Mater. 1 (2017) 2.
[27] A.B. Farimani, K. Min, N.R. Aluru, ACS Nano 8 (2014) 7914.
[28] D. Sarkar, W. Liu, X. Xie, A.C. Anselmo, S. Mitragotri, K. Banerjee, ACS Nano 8 (2014) 3992.
[29] F.K. Perkins, A.L. Friedman, E. Cobas, P. Campbell, G. Jernigan, B.T. Jonker, Nano Lett. 13 (2013) 668.
[30] B. Cho, J. Yoon, S.K. Lim, A.R. Kim, D.-H. Kim, S.-G. Park, J.-D. Kwon, Y.-J. Lee, K.-H. Lee, B.H. Lee, et al., ACS Appl. Mater. Interfaces 7 (2015) 16775.
[31] D.J. Late, Y.-K. Huang, B. Liu, J. Acharya, S.N. Shirodkar, J. Luo, A. Yan, D. Charles, U.V. Waghmare, V.P. Dravid, et al., ACS Nano 7 (2013) 4879.
[32] H. Li, G. Lu, Y. Wang, Z. Yin, C. Cong, Q. He, L. Wang, F. Ding, T. Yu, H. Zhang, Small 9 (2013) 1974.
[33] Y. Nakata, T. Yoshizawa, K. Sugawara, Y. Umemoto, T. Takahashi, T. Sato, A.C.S. Appl, Nano Mater. 1 (2018) 1456.
[34] Z. Yan, C. Jiang, T. Pope, C. Tsang, J. Stickney, P. Goli, J. Renteria, T. Salguero, A. Balandin, J. Appl. Phys. 114 (2013) 204301.
[35] A. Castellanos-Gomez, E. Navarro-Moratalla, G. Mokry, J. Quereda, E. Pinilla-Cienfuegos, N. Agraït, H.S. Van Der Zant, E. Coronado, G.A. Steele, G. Rubio-Bollinger, Nano Res. 6 (2013) 191.
[36] H. Ryu, Y. Chen, H. Kim, H.-Z. Tsai, S. Tang, J. Jiang, F. Liou, S. Kahn, C. Jia, A.A. Omrani, et al., Nano Lett. 18 (2018) 689.
[37] R.R. Nair, W. Ren, R. Jalil, I. Riaz, V.G. Kravets, L. Britnell, P. Blake, F. Schedin, A.S. Mayorov, S. Yuan, et al., Small 6 (2010) 2877.
[38] T. Sainsbury, M. Passarelli, M. Naftaly, S. Gnaniah, S.J. Spencer, A.J. Pollard, ACS Appl. Mater. Interfaces 8 (2016) 4870.
[39] V. Sreepal, M. Yagmurcukardes, K.S. Vasu, D.J. Kelly, S.F. Taylor, V.G. Kravets, Z. Kudrynskyi, Z.D. Kovalyuk, A. Patanè, A.N. Grigorenko, et al., Nano Lett. 19 (2019) 6475.
[40] G.-H. Kim, H. Jang, Y.J. Yoon, J. Jeong, S.Y. Park, B. Walker, I.-Y. Jeon, Y. Jo, H. Yoon, M. Kim, et al., Nano Lett. 17 (2017) 6385.
[41] L. Li, R. Qin, H. Li, L. Yu, Q. Liu, G. Luo, Z. Gao, J. Lu, ACS Nano 5 (2011) 2601.
[42] L. Ries, E. Petit, T. Michel, C.C. Diogo, C. Gervais, C. Salameh, M. Bechelany, S. Balme, P. Miele, N. Onofrio, et al., Nat. Mater. 18 (2019) 1112.
[43] W. Hirunpinyopas, E. Prestat, S.D. Worrall, S.J. Haigh, R.A. Dryfe, M.A. Bissett, ACS Nano 11 (2017) 11082.
[44] J. Zhao, C.R. Cabrera, Z. Xia, Z. Chen, Carbon 104 (2016) 56.
[45] Y. Li, Z. Zhu, J. Yu, B. Ding, ACS Appl. Mater. Interfaces 7 (2015) 13538.
[46] M. Yagmurcukardes, C. Bacaksiz, R. Senger, H. Sahin, 2D Mater. 4 (2017) 035013.
[47] J.O. Sofo, A.S. Chaudhari, G.D. Barber, Phys. Rev. B 75 (2007) 153401.
[48] M.S. Fuhrer, C.N. Lau, A.H. MacDonald, MRS Bull. 35 (2010) 289.
[49] T. Wehling, K. Novoselov, S. Morozov, E. Vdovin, M. Katsnelson, A. Geim, A. Lichtenstein, Nano Lett. 8 (2008) 173.
[50] J.T. Robinson, J.S. Burgess, C.E. Junkermeier, S.C. Badescu, T.L. Reinecke, F.K. Perkins, M.K. Zalalutdniov, J.W. Baldwin, J.C. Culbertson, P.E. Sheehan, et al., Nano Lett. 10 (2010) 3001.
[51] Z. Kahraman, M. Yagmurcukardes, H. Sahin, J. Mater. Res. 35 (2020) 1397–1406.
[52] A.-Y. Lu, H. Zhu, J. Xiao, C.-P. Chuu, Y. Han, M.-H. Chiu, C.-C. Cheng, C.-W. Yang, K.-H. Wei, Y. Yang, et al., Nat. Nanotechnol. 12 (2017) 744.
[53] A. Kandemir, H. Sahin, Phys. Rev. B 97 (2018) 155410.
[54] J. Zhang, S. Jia, I. Kholmanov, L. Dong, D. Er, W. Chen, H. Guo, Z. Jin, V.B. Shenoy, L. Shi, et al., ACS Nano 11 (2017) 8192.
[55] L. Dong, J. Lou, V.B. Shenoy, ACS Nano 11 (2017) 8242.
[56] Z. Kahraman, A. Kandemir, M. Yagmurcukardes, H. Sahin, J. Phys. Chem. C 123 (2019) 4549.
[57] Y. Cheng, Z. Zhu, M. Tahir, U. Schwingenschlögl, EPL (Europhys. Lett.) 102 (2013) 57001.
[58] J.P. Perdew, K. Burke, M. Ernzerhof, Phys Rev. Lett. 77 (1996) 3865.
[59] G. Kresse, J. Furthmüller, Phys. Rev. B 54 (1996) 11169.
[60] S. Grimme, J. Comput. Chem. 27 (2006) 1787.
[61] J. Heyd, G.E. Scuseria, M. Ernzerhof, J. Chem. Phys. 118 (2003) 8207.
[62] G. Henkelman, A. Arnaldsson, H. Jónsson, Comput. Mater. Sci. 36 (2006) 354.
[63] A. Togo, F. Oba, I. Tanaka, Phys. Rev. B 78 (2008) 134106.
[64] D.C. Elias, R.R. Nair, T. Mohiuddin, S. Morozov, P. Blake, M. Halsall, A.C. Ferrari, D. Boukhvalov, M. Katsnelson, A. Geim, et al., Science 323 (2009) 610.
[65] R.R. Nair, W. Ren, R. Jalil, I. Riaz, V.G. Kravets, L. Britnell, P. Blake, F. Schedin, A.S. Mayorov, S. Yuan, et al., Small 6 (2010) 2877.
[66] R. Frisenda, M. Drüppel, R. Schmidt, S.M. de Vasconcellos, D.P. de Lara, R. Bratschitsch, M. Rohlfing, A. Castellanos-Gomez, NPJ 2D Mater. Appl. 1 (2017) 1.
[67] C. Androulidakis, E.N. Koukaras, G. Paterakis, G. Trakakis, C. Galiotis, Nat. Commun. 11 (2020) 1.
[68] H. Sahin, Phys. Rev. B 92 (2015) 085421.